Electronic Supplementary Material (ESI) for Journal of Materials Chemistry C.

Supplementary Material

Rational design of thermally activated delayed fluorescence emitters with aggregation-induced emission employing combined charge transfer pathways for efficient non-doped OLEDs

Fulong Ma[a], Yu Cheng[a], Yu Zheng[a], Hefang Ji[a], Kamvan Hasrat[a], Zhengjian Qi[a*]

[a]Jiangsu Province Hi-Tech Key Laboratory for Biomedical Research, School of Chemistry and Chemical Engineering, Southeast University, Nanjing, Jiangsu 211189, PR China

Contents

1. Calculation of rate constants

$$k_{r,\ S} = \frac{\Phi_p}{\tau_p} \qquad (1)$$

$$k_{nr,\ S} = k_{r,\ S}\left(\frac{1 - \Phi_{PL}}{\Phi_{PL}}\right) \qquad (2)$$

$$k_{ISC} = k_{r,\ S}\left(\frac{1}{\Phi_p} - \frac{1}{\Phi_{PL}}\right) \qquad (3)$$

$$k_{RISC} = \frac{\Phi_{PL}}{k_{r,\ S}\,\tau_p\,\tau_d} \qquad (4)$$

$$\Phi_{p=}\frac{A_1\tau_p}{A_1\tau_p + A_{21}\tau_d}\Phi_{PL} \qquad (5)$$

$$\Phi_{d\,=}\frac{A_2\tau_d}{A_1\tau_p + A_2\tau_d}\Phi_{PL} \qquad (6)$$

The rate constants were calculated according to above equation (1)-(6): Where τ_p and τ_d were the lifetimes of the prompt and delayed decay components, respectively. Φ_{PL} and Φ_p were the total PL quantum yield, prompt fluorescence and delayed fluorescence quantum yield, respectively. $k_{r,\ S}$, $k_{nr,\ S}$, k_{ISC} and k_{RISC} were the rate constant for fluorescence radiative transition, non-radiative transition, intersystem crossing (ISC) and reverse intersystem crossing (RISC) processes, respectively. A_1 and A_2 were the frequency factors according to the followed fitting model of transient PL decay curves : $I(t) = A_1 \exp\left(-\frac{t_1}{\tau_p}\right) + A_2 \exp\left(-\frac{t_2}{\tau_d}\right)$.

2. Photophysical properties

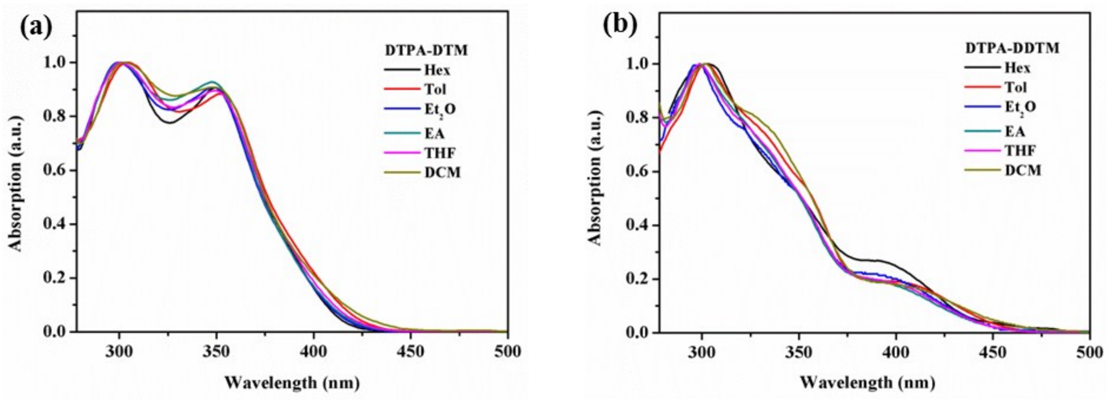

Fig. S1 The UV-vis absorption spectra of of DTPA-DTM (a) and DTPA-DDTM (b) in different solvents at room temperature.

Table S1. Photophysical properties of DTPA-DTM and DTPA-DDTM in solvents with different polarity.

Solvent	DTPA-DTM			DTPA-DDTM		
	$\lambda_{abs, max}$ (nm)	$\lambda_{em, max}$ (nm)	Stokes shift (cm^{-1})	$\lambda_{abs, max}$ (nm)	$\lambda_{em, max}$ (nm)	Stokes shift (cm^{-1})
Hex	349	445	6181	393	498	5364
Tol	353	474	7231	405	533	5929
Et_2O	348	471	7504	397	542	6738
EA	347	494	8575	404	561	6927
THF	349	497	8532	404	567	7115
DCM	349	538	10065	405	605	8162

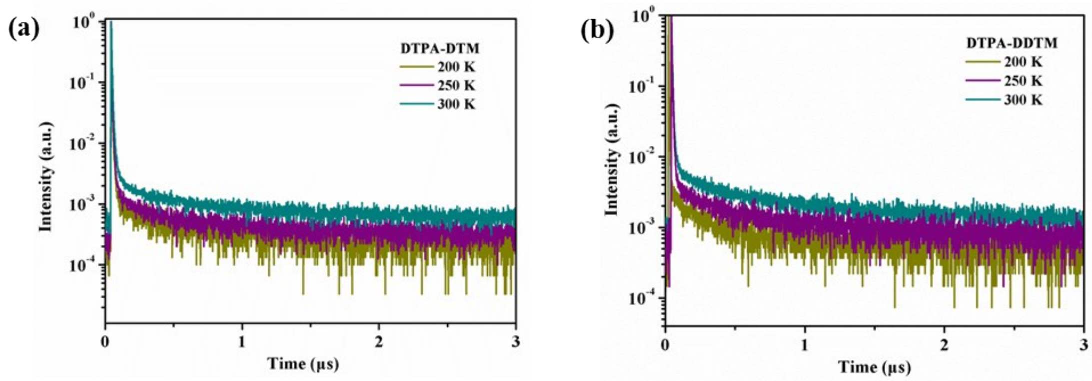

Fig. S2 The transient PL decay spectra of DTPA-DTM (a) and DTPA-DDTM (b) in neat films under nitrogen at different temperatures.

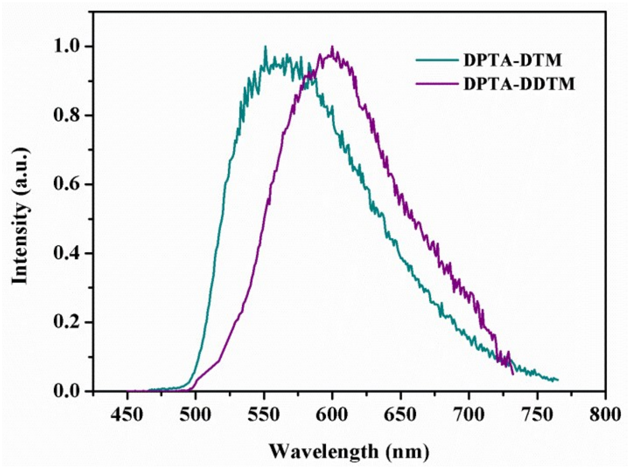

Fig. S3 Phosphorescence spectra measured at 77 K in neat film states.

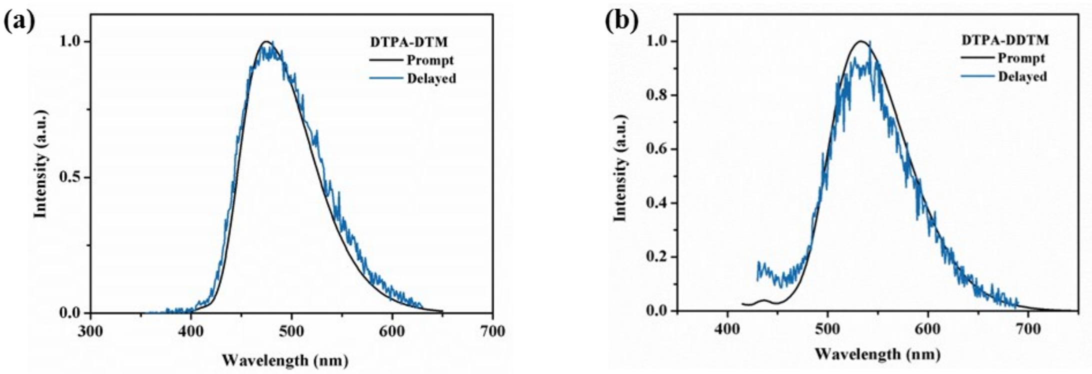

Fig. S4 Prompt and delayed (5 us) spectra of DTPA-DTM (a) and DTPA-DDTM (b) measured in toluene under nitrogen at room temperature.

3. X-ray crystallographic data

Table S2. Crystal data and structure refinement for DTPA-DDTM.

Empirical formula	$C_{68}H_{44}N_2$O2S2
CCDC No.	1915211
Temperature (K)	193(2)
Crystal system	Monoclinic
Space group	C 1 2/c 1
a (Å)	24.5727(13)
b (Å)	11.4734(5)
c (Å)	23.3323(11)
α (°)	90
β (°)	98.189(2)
γ (°)	90
V (Å^3)	6511.1(5)
Z	4

Density (calculated)	1.005
F(000)	2056.0
Crystal size (mm)	0.100×0.200×0.200
Absorption coefficient (mm^{-1})	0.682
Theta range for data collection (°)	3.16 to 57.09
Index ranges	-30<=h<=30, -14<=k<=14, -29<=l<=29
Reflections collected	47973
Independent reflections	6660 [R(int) = 0.0835]
Absorption correction	Multi-Scan
Max. and min. transmission	0.9350 and 0.8760
Refinement method	Full-matrix least-squares on F^2
Data / restraints / parameters	6660 / 0 / 334
Goodness-of-fit on F^2	1.046
Final R indices [I>2sigma(I)]	R1 = 0.0493, wR2 = 0.1309
R indices (all data)	R1 = 0.0778, wR2 = 0.1463
Largest diff. peak and hole	0.253 and -0.337 eÅ^{-3}

4. Optimized molecular structures and the measured distance

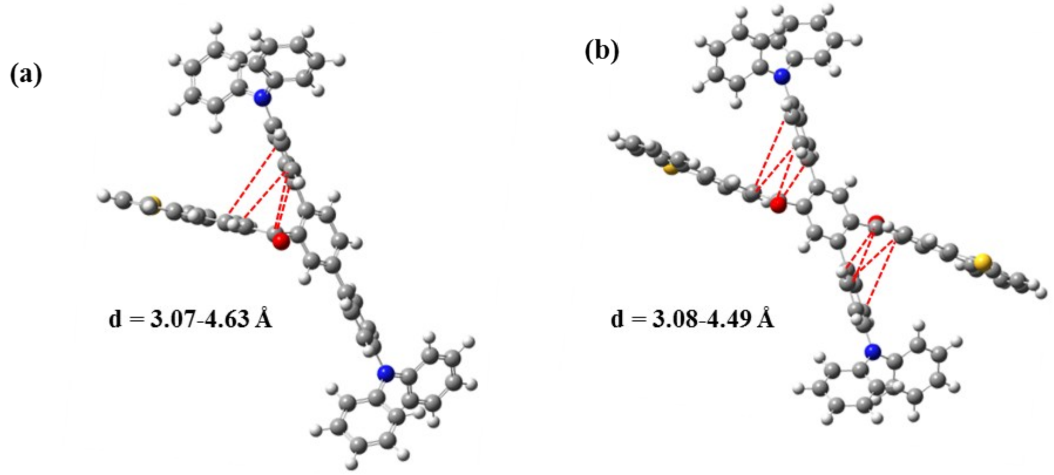

Fig. S5 The optimized molecular structures and the distance measured by Gaussview 5.0 of DTPA-DTM (a) and DTPA-DDTM (b).

5. Cyclic voltammogram

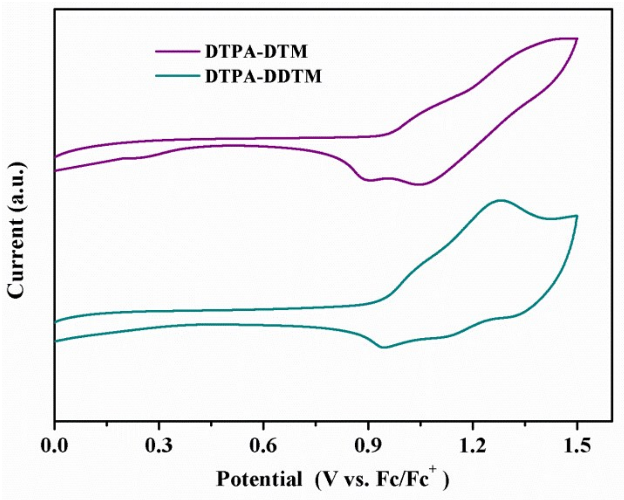

Fig. S6 Cyclic voltammogram of DTPA-DTM and DTPA-DDTM.

6. Device fabrication and characterization

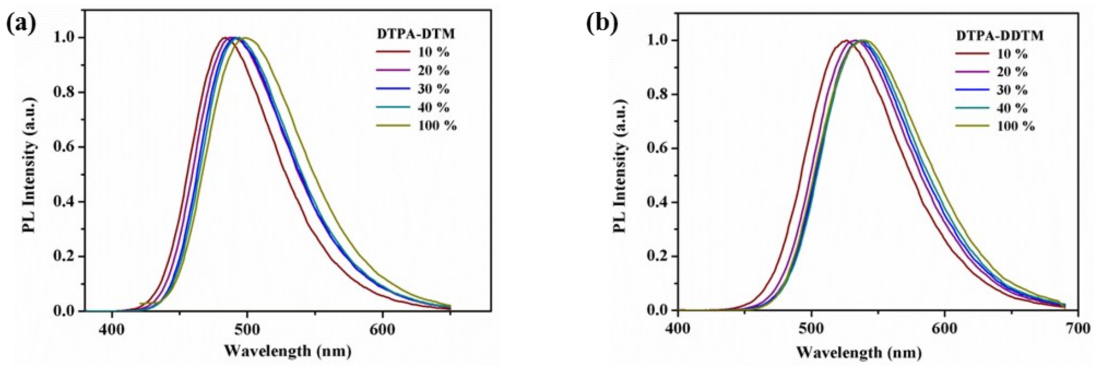

Fig. S7 The PL spectra of DTPA-DTM and DTPA-DDTM with different doping concentrations.

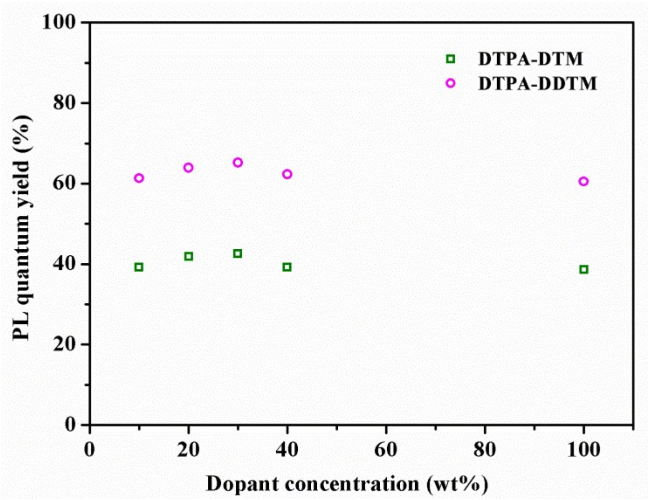

Fig. S8 The PL quantum yield of DTPA-DTM and DTPA-DDTM with different doping concentrations.

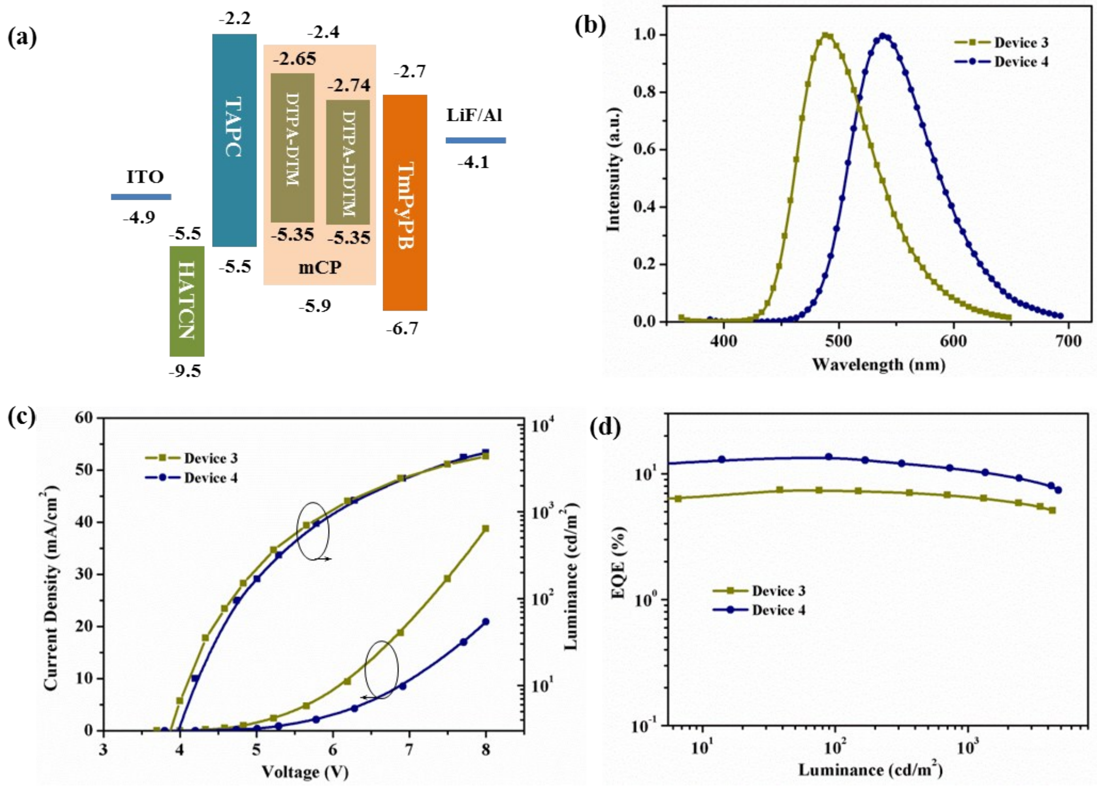

Fig. S9 (a) Energy diagram of the materials used in the doped devices; (b) normalized EL spectral; (c) current density-voltage-luminance (J-V-L) curves; (d) EQE versus luminance curves.

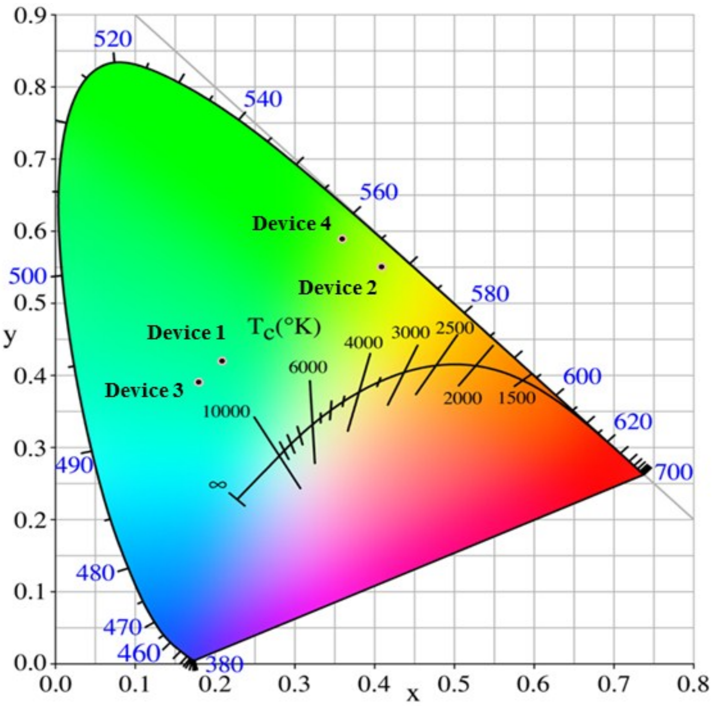

Fig. S10. CIE diagram of the devices based on DTPA-DTM and DTPA-DDTM.

Table S3. Maximum emission peak and PLQYs of DTPA-DTM and DTPA-DDTM in mCP host with different doping concentrations.

Compound	Conc[a] [wt%]	10	20	30	40	100
DTPA-DTM	λ_{em}[b] [nm]	480	487	491	493	498
	ϕ_{F}[c] [%]	39.5	41.9	42.5	39.2	38.6
DTPA-DDTM	λ_{em}[b] [nm]	527	532	537	538	539
	ϕ_{F}[c] [%]	61.3	63.9	65.2	62.3	60.5

[a]Dopant concentration in emitter:mCP codeposited thin films.

[b]Maximum emission peak measured at 300 K.

[c]Absolute PL quantum yield measured using an integrating sphere under N_2 at 300 K.

7. ^{1}H NMR and ^{13}C NMR spectra

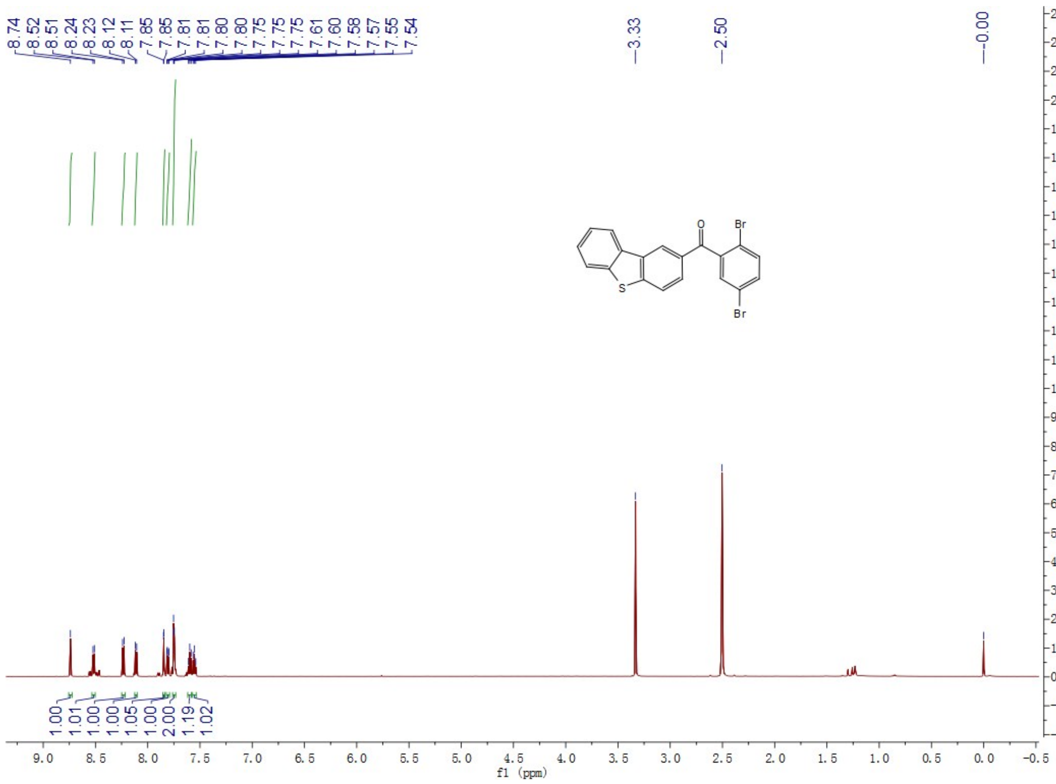

^{1}H-NMR spectrum of DBr-DTM in DMSO-*d6*

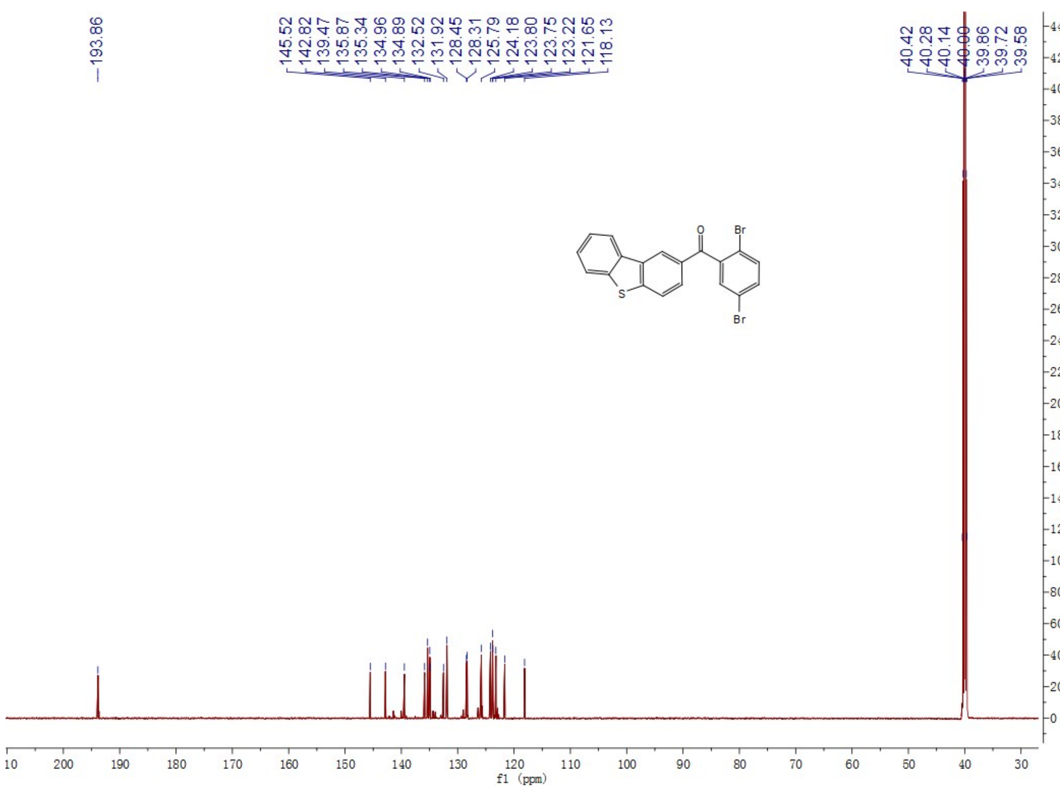

^{13}C-NMR spectrum of DBr-DTM in DMSO-*d6*

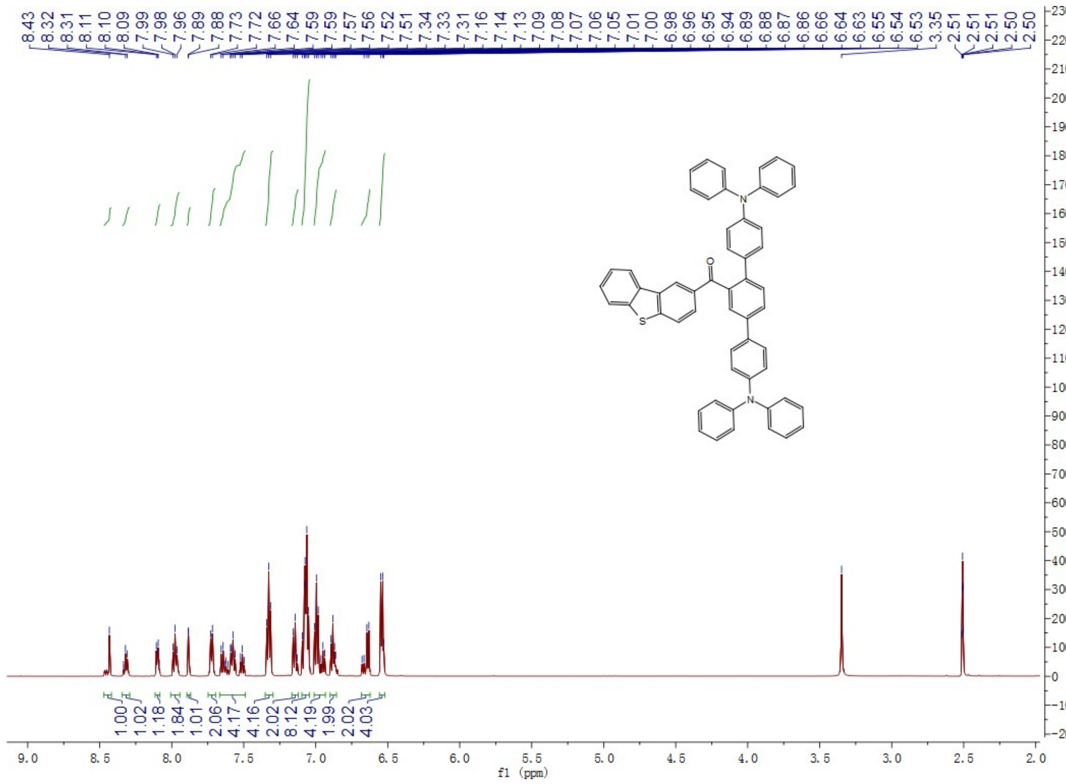

^{1}H-NMR spectrum of DTPA-DTM in DMSO-*d*6

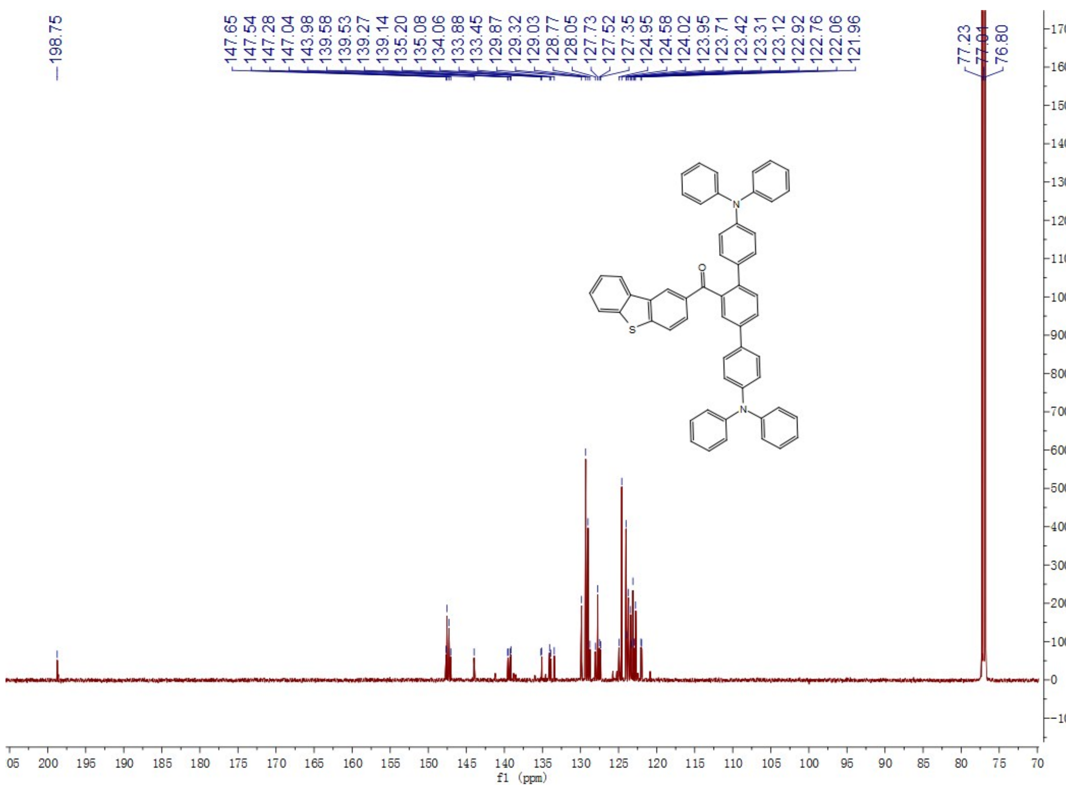

^{13}C-NMR spectrum of DTPA-DTM in DMSO-*d*6

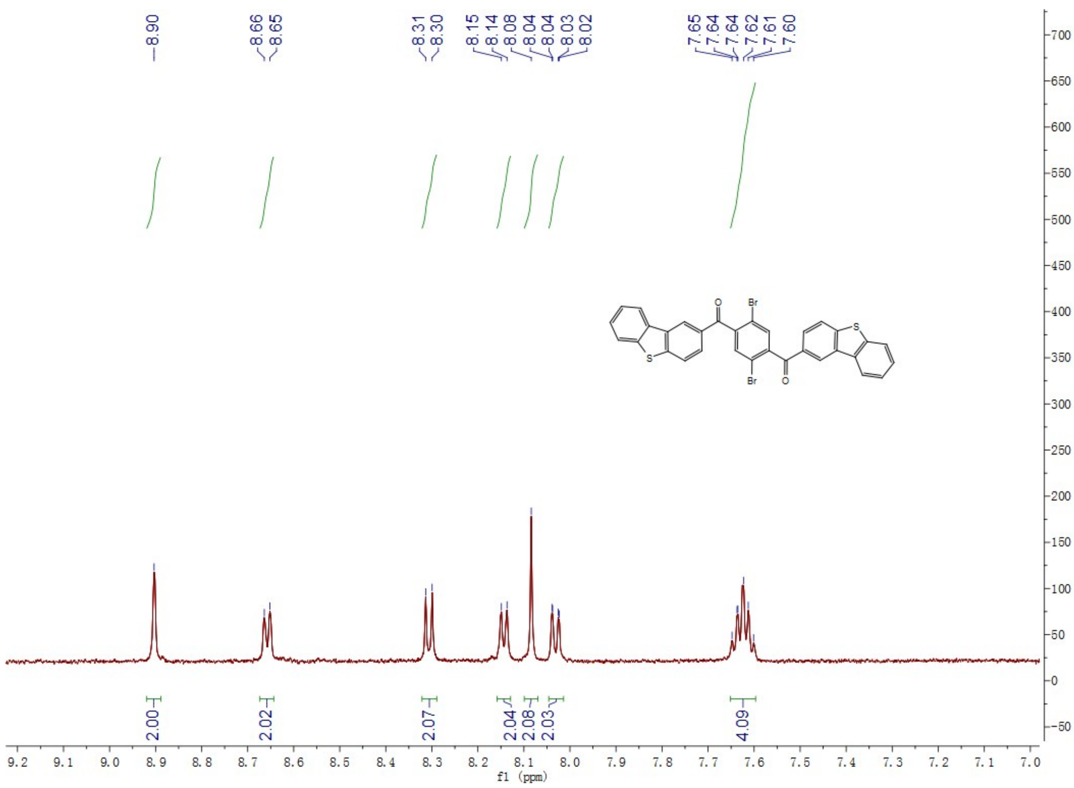

^{1}H-NMR spectrum of DBr-DDTM in $CDCl_3$

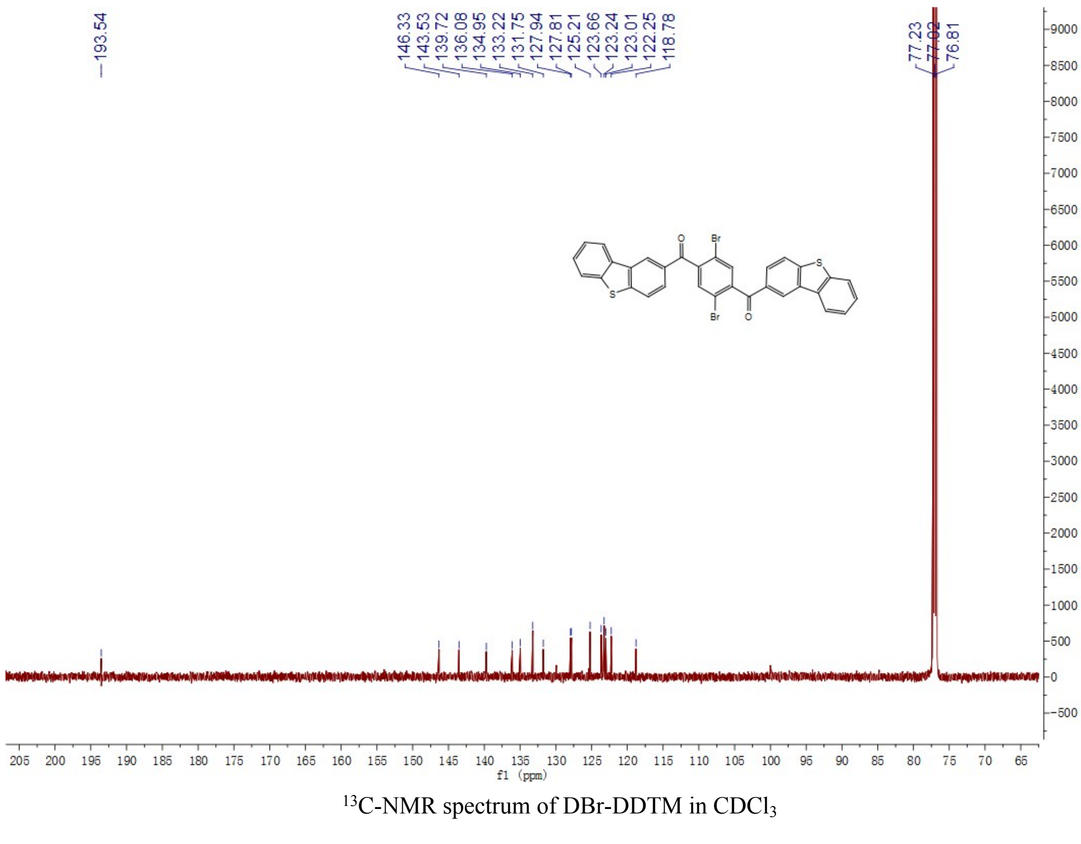

^{13}C-NMR spectrum of DBr-DDTM in $CDCl_3$

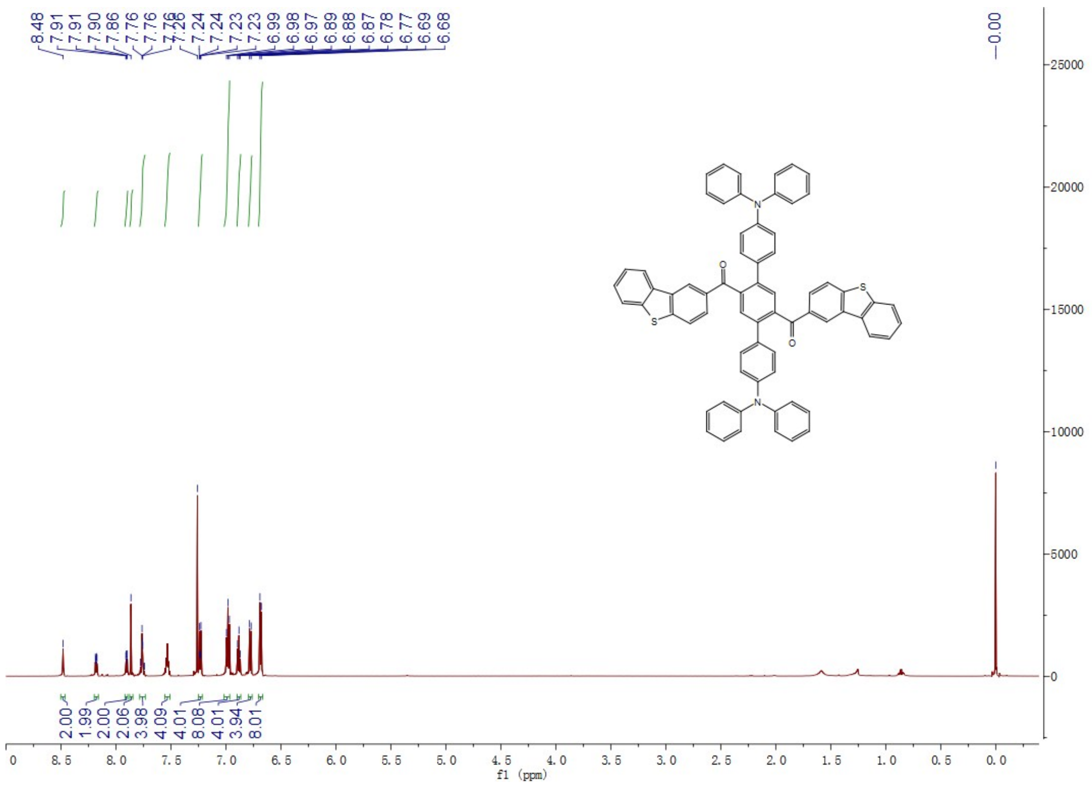

[1]H-NMR spectrum of DTPA-DDTM in $CDCl_3$

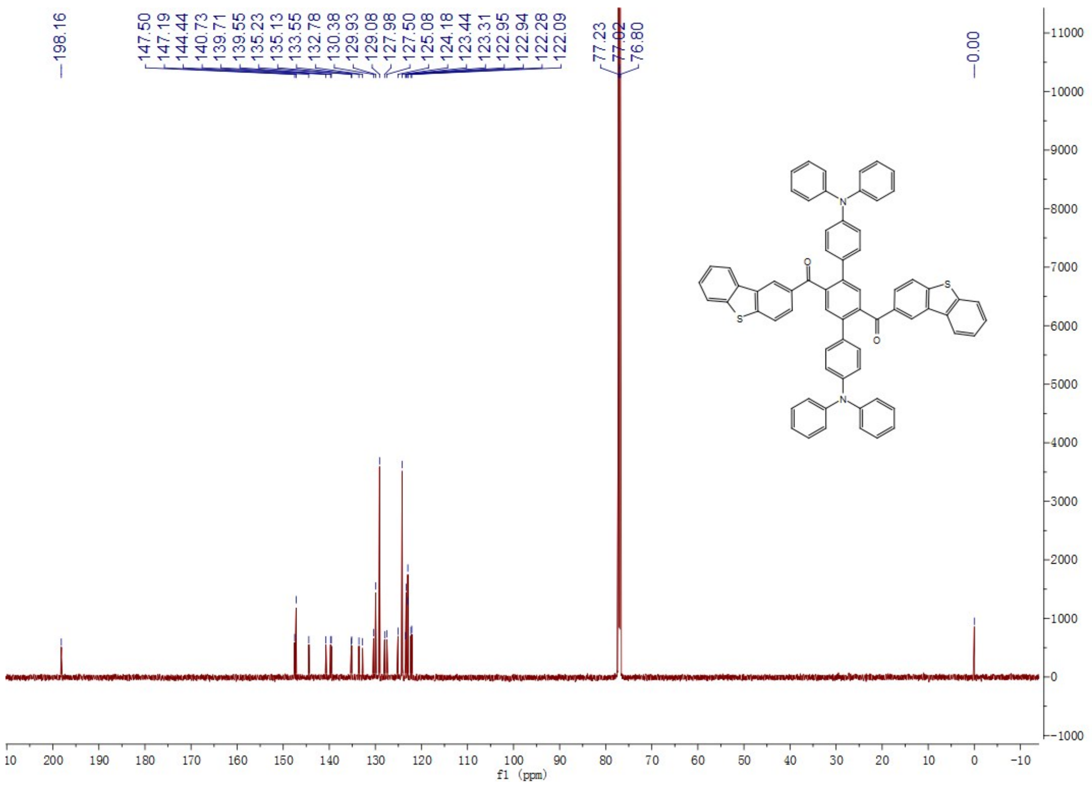

[13]C-NMR spectrum of DTPA-DDTM in $CDCl_3$

8. LC-MS and MALDI-TOF spectra

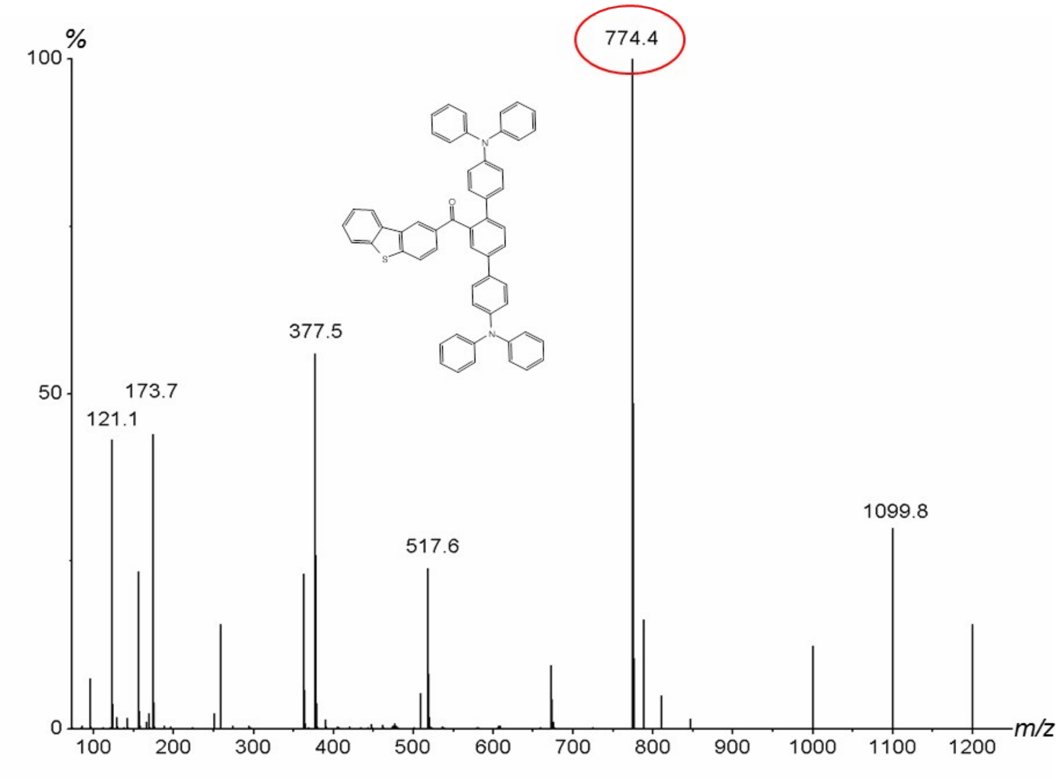

LC-MS spectrum of DTPA-DTM in CH_3CN

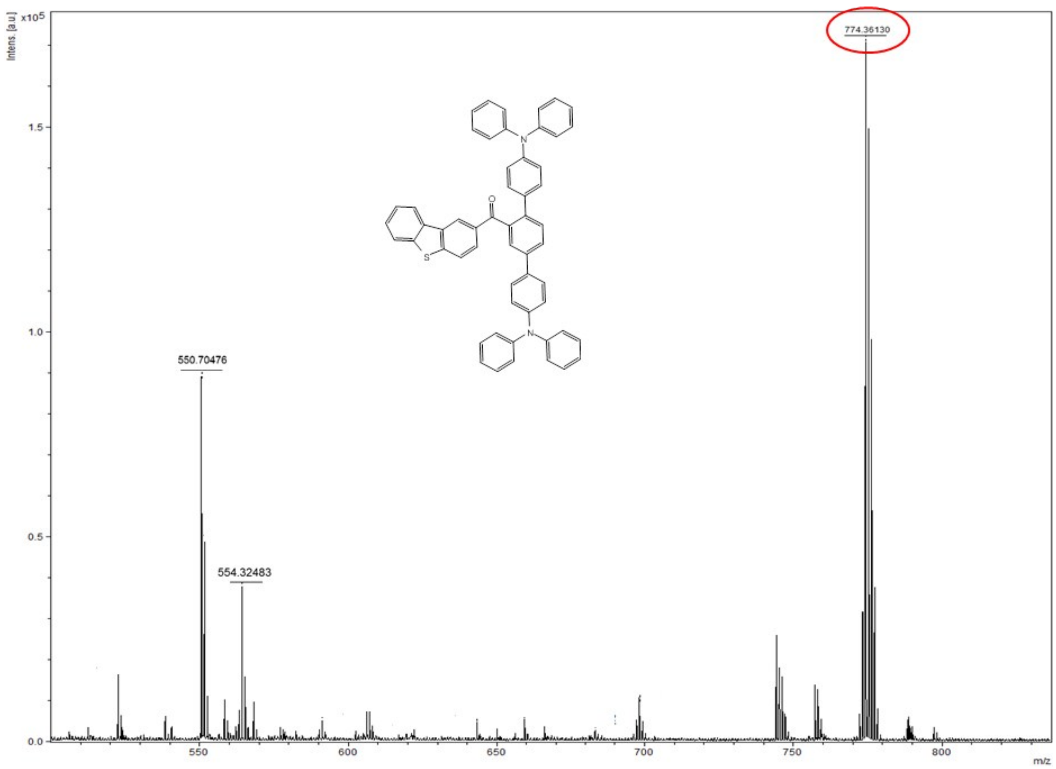

MALDI-TOF spectrum of DTPA-DTM in THF

LC-MS spectrum of DTPA-DDTM in CH_3CN

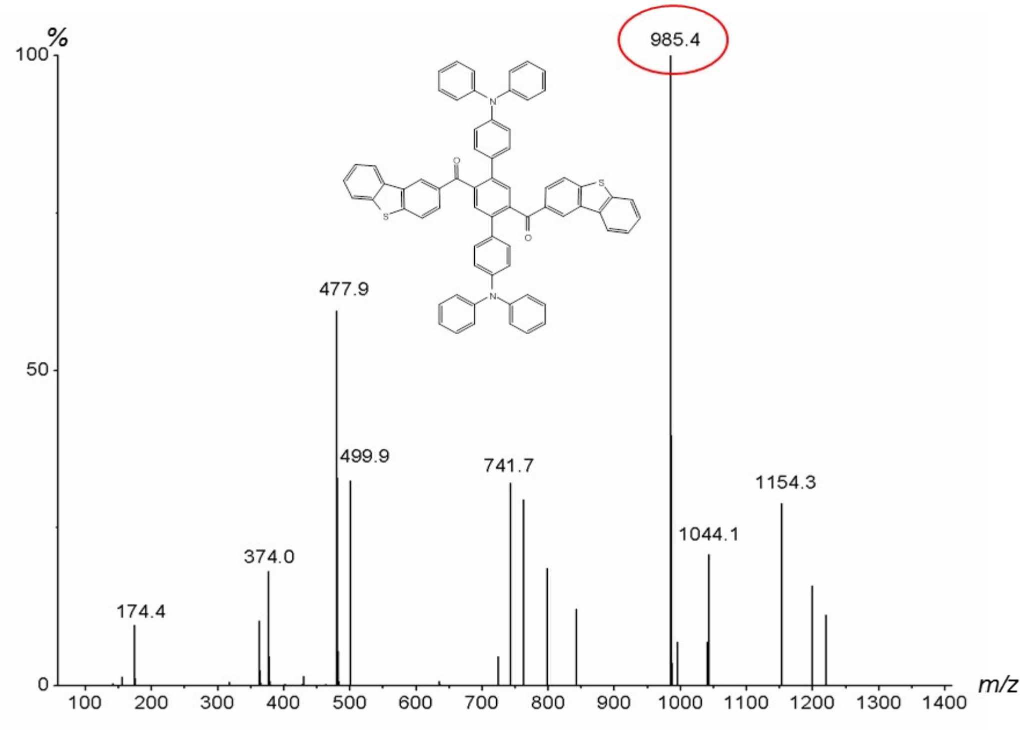

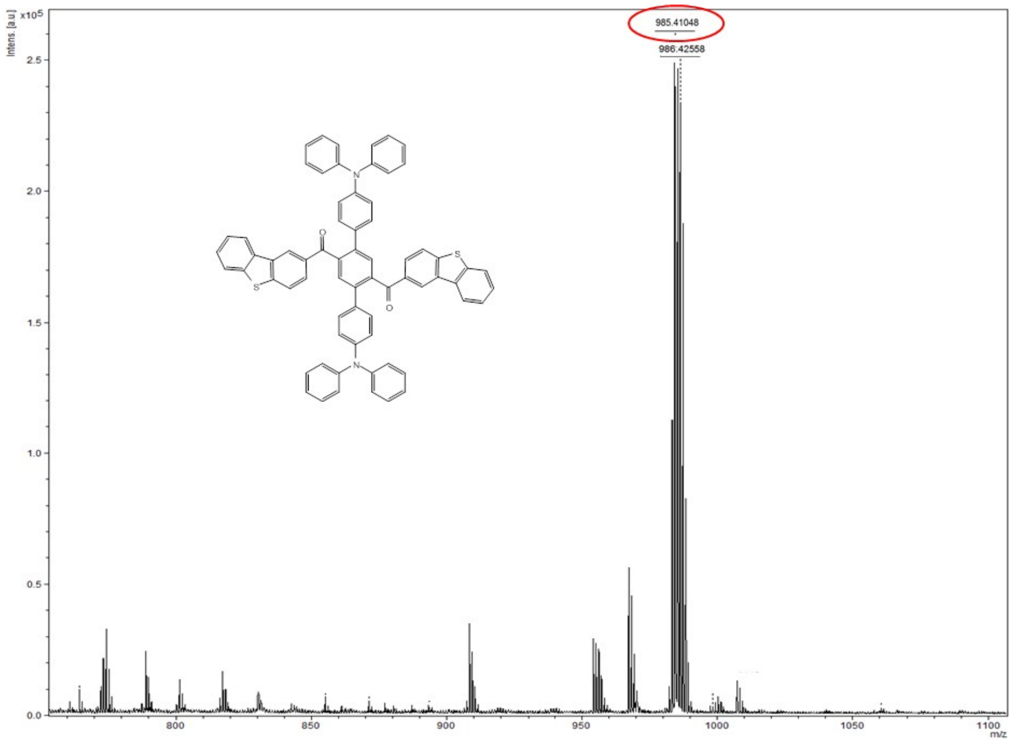

MALDI-TOF spectrum of DTPA-DDTM in THF